ISSN 1063-7842, Technical Physics, 2011, Vol. 56, No. 5, pp. 656–661. © Pleiades Publishing, Ltd., 2011.
Original Russian Text © A.S. Parshin, S.A. Kushchenkov, G.A. Aleksandrova, S.G. Ovchinnikov, 2011, published in Zhurnal Tekhnicheskoĭ Fiziki, 2011, Vol. 81, No. 5, pp. 69–74.

SOLID STATE ELECTRONICS

New Opportunities for Quantitative Analysis as Applied to Reflected Electron Energy Loss Spectroscopy of Fe/Si Structures

A. S. Parshin[a, b]*, S. A. Kushchenkov[a], G. A. Aleksandrova[a], and S. G. Ovchinnikov[b]

[a] *Reshetnev Siberian State Aerospace University, pr. im. Gazety Krasnoyarskii Rabochii 31, Krasnoyarsk, 660014 Russia*
**e-mail: aparshin@sibsau.ru*

[b] *Kirenskii Institute of Physics, Siberian Branch, Russian Academy of Sciences, Akademgorodok, Krasnoyarsk, 660036 Russia*

Received June 24, 2010; in final form, October 13, 2010

Abstract—The feasibility of determining the elemental composition, chemical state, and element distribution across the depth in a subsurface region using the computer simulation of the electron inelastic scattering cross section is demonstrated with iron layers on silicon substrates. Analysis is carried out based on the dielectric theory and on the experimental determination of the product of the electron inelastic mean free path by the inelastic scattering cross section from reflected electron energy loss spectra.

DOI: 10.1134/S1063784211050264

INTRODUCTION

Metal-on-semiconductor nanostructures are routinely characterized by electron spectroscopy methods, such as photoelectron spectroscopy, Auger electron spectroscopy, and characteristic electron energy loss spectroscopy. Owing to a recent tendency toward electron device miniaturization, interest has quickened in growth mechanisms of low-dimensional magnetic structures, namely, quantum wires and quantum dots.

Investigation into Fe/Si nanostructures is associated first of all with application of these materials in microelectronic, nanoelectronic, and spintronic devices. Because of fast interdiffusion of iron and silicon atoms, different semiconducting, dielectric, and/or magnetic silicides arise in these structures depending on growth conditions [1–6]. A variety of iron–silicon compounds forming in the course of growth of iron nanostructures on silicon suggests that this process is very complicated and inconstant, so that the need for new techniques to examine the physicochemical properties and structure of these and related materials becomes obvious.

In this work, we elaborate upon the method [7] of determining the atomic concentration of elements in a Fe_xSi_{1-x} system from the maxima of the electron inelastic scattering cross section. Using these data, one can find the elemental composition and thickness of the iron film and interface by computer simulation of the electron inelastic scattering cross section in layered structures.

EXPERIMENT

Iron films were grown on single-crystalline Si(100) substrates by thermal evaporation in ultrahigh vacuum. Growth conditions (substrate temperature and the amount of iron arrived at the substrate for the growth time) were varied so as to provide different distributions of the elements in a subsurface layer of the structure due to the interdiffusion of iron and silicon atoms and the formation of various iron silicides. For each substrate temperature, the growth rate of the iron film was the same, 0.2 nm/min, so that the effective thickness of the film for an evaporation time of 10 min reached 2 nm. At a substrate temperature of 620°C, we prepared two additional samples: in one of which the effective thickness of the iron film was 0.1 nm, and in the other an iron film was deposited on a silicon sublayer covering the substrate.

Reflected electron energy loss (REEL) spectra were recorded in situ with a 09IOS-03 electron spectrometer built in an ultrahigh-vacuum multi-module processing facility [8]. The REEL spectra were recorded in differential form for a primary electron energy of 1200 eV. To determine the energy losses corresponding to peaks in the spectrum, experimental curves were numerically differentiated. In this case, the energy losses correlate with maxima in the curves $-d^2N/dE^2$ (N is the number of electrons with energy E).

After subtracting the instrument function from experimental REEL spectra and numerically integrating them with the QUASES™ XS REELS (QUantitative Analysis of Surfaces by Electron Spectroscopy, cross sections determined by REELS) [9] program package, we found the product of electron inelastic mean free path λ by differential inelastic scattering

Table 1. Growth conditions and plasmon energies in the samples

No.	Sample	Substrate temperature, °C	Evaporation time, min	Plasmon energy, eV	Note
1	Fe	20	–	22.3 ± 0.2	
2	*A*	20	10	20.7 ± 0.2	
3	*B*	270	10	21.0 ± 0.2	
4	*C*	620	10	17.2 ± 0.1	
5	*D*	620	10	17.1 ± 0.2	Silicon sublayer
6	*E*	620	0.5	17.2 ± 0.1	
7	Si	20	–	17.0 ± 0.1	

cross section $K(E_0, E_0 - E)$, where E_0 is the energy of elastically scattered electrons. The computational algorithm is given in [10],

$$\lambda K(E_0, E_0 - E) = \frac{1}{c}\left[j(E) - \int_E^{E_0} \lambda K(E_0, E' - E) j(E') dE'\right], \quad (1)$$

where $j(E)$ is an experimental spectrum and c is the area under the elastic peak.

RESULTS AND DISCUSSION

Growth conditions for seven Fe/Si(100) systems are listed in Table 1.

A reference REEL spectrum for iron was taken of sample 1 (an iron film about 50 nm thick grown by room-temperature evaporation on a silicon substrate in ultrahigh vacuum). In this case, Auger and REEL spectra were the same as those taken of bulk iron. A spectrum taken of a pure Si(100) substrate (sample 7) was used as a reference spectrum for silicon.

Figure 1 shows differential REEL spectra normalized to the elastic peak for the test and reference samples (the energy of primary electrons was 1200 eV). The spectrum of the sample grown at 620°C contains a peak of electron energy multiple losses due to the excitation of volume plasmons. The plasmon energy averaged over all energy loss peaks are listed in Table 1 (the plasmon energies were determined by the repeated differentiation of the differential loss spectra). The spectrum of sample *A* obtained at room temperature is similar to the spectrum of bulk iron except for the volume plasmon energy. In this sample, the energy of volume plasmons, being 1.6 eV lower than in bulk iron, is close to published data for the volume plasmon energy in iron silicides [1, 11]. The spectrum of sample *A* exhibits a noticeable peak at 57.5 eV, which resembles the peak of band-to-band transition M_{23} in iron (55.5 eV) [1]. In the spectrum of sample *B* obtained at a substrate temperature of 270°C, peaks due to multiple plasmons stand out and their energy is also close to that typical of iron silicides. Samples *C*, *D*, and *E* grown at the same substrate temperature (620°C) differ either in the amount of deposited iron (*C, E*) or in the presence of the additional silicon sublayer (*C, D*). Their spectra are similar to that of pure silicon and show many multiple loss peaks. Note that the loss peak height increases with growth temperature, because the electron inelastic scattering cross section grows from sample *A* to sample *E*.

To quantitatively characterize the variation of the electron inelastic scattering cross section in the samples, we calculated the product of the electron inelastic mean free path by the inelastic energy loss cross section, $\hbar\omega$: $\lambda K(\hbar\omega)$ (Fig. 2), using the QUASES^{TM} XS REELS program package.

The product $\lambda K_{max}(\hbar\omega)$ characterizes the probability of electron energy losses over the inelastic mean free path per unit energy. Since the basic mechanism through which electrons lose energy in collisions with a solid is the plasmon excitation, a maximum in the inelastic energy loss cross section corresponds to the energy of volume plasmon excitation. The loss rate is determined by the maximum of the product of the electron inelastic mean free path by the inelastic scattering cross section. It is seen from the above results that the maximum of $\lambda K_{max}(\hbar\omega)$ in the Fe/Si system is

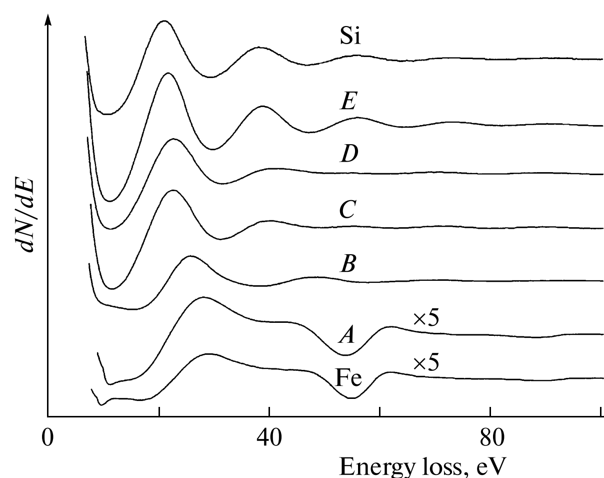

Fig. 1. Differential loss spectra for the reflected electron energy (the primary electron energy is 1200 eV).

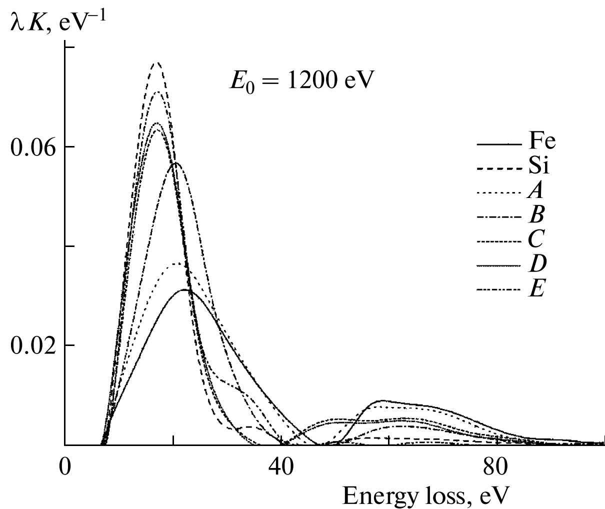

Fig. 2. Spectrum of the inelastic scattering energy loss cross section.

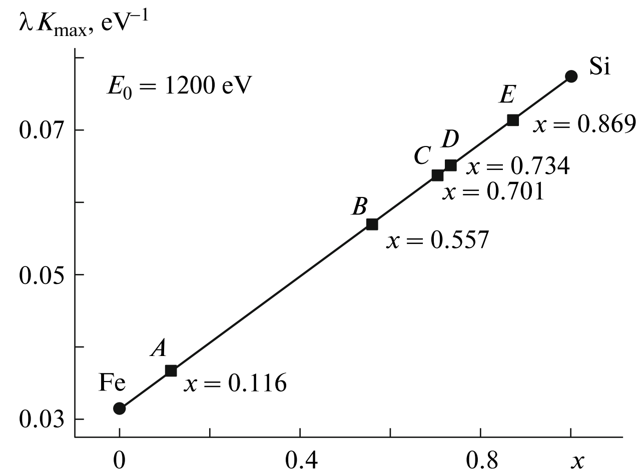

Fig. 3. Determination of the silicon atomic concentration in the Si_xFe_{1-x} system.

more sensitive to growth conditions and, hence, to a change in the composition and chemical state of the samples than to a change in energy losses.

To treat the results on a quantitative basis, we used the technique [7] for determining the atomic concentration of elements in the Fe/Si system from an experimentally found linear dependence of the maximum of the product of the electron inelastic mean free path by the electron inelastic scattering cross section in this system.

Figure 3 plots the silicon concentration in a Si_xFe_{1-x} system calculated from a calibration curve constructed based on experimental data for the reference Fe ($x = 0$) and Si ($x = 1$) samples. Filled squares are experimental values of $\lambda K_{max}(\hbar\omega)$ for the samples (Fig. 2). To each data point, there corresponds an effective (without regard to the element distribution across the depth) silicon concentration. Table 2 lists loss maxima and the atomic and volume concentrations of silicon.

Table 2. Composition of the Si_xFe_{1-x} structure

No.	Sample	λK_{max}, eV^{-1}	Atomic concentration, x	Volume fraction, ν
1	Fe	0.0315	0	0
2	*A*	0.0368	0.116	0.182
3	*B*	0.0570	0.557	0.681
4	*C*	0.0636	0.701	0.799
5	*D*	0.0651	0.734	0.824
6	*E*	0.0713	0.869	0.918
7	Si	0.0773	1	1

The element distribution across the depth of the structures was described with computer simulation in terms of the dielectric response theory as applied to the electron inelastic scattering cross section in layered structures. Here, we elaborate upon the Yubero–Tougaard model and computational technique [12] for interaction between electrons and a semi-infinite medium that is characterized by a complex dielectric function of the wavenumber and frequency, $\varepsilon(k, \omega)$. The algorithm suggested by us for computing the electron inelastic scattering cross section based on the dielectric response theory in bilayer (film/substrate) structures with a sharp interface is given in [13]. In this work, the contribution to the inelastic scattering cross section for electrons scattered at depth a from the surface of the bilayer structure (Fig. 4) is given by

$$K_{sc}(E_0, \hbar\omega) = \frac{1}{\lambda_{eff}^2}\int_0^d 2a\exp(-2a/\lambda_{eff})K_{eff}^{film}(E_0, \hbar\omega, a)da + \frac{1}{\lambda_{eff}^2}\int_d^\infty 2a\exp(-2a/\lambda_{eff})K_{eff}^{subs}(E_0, \hbar\omega, a)da. \quad (2)$$

Here, d is the thickness of the film; K_{eff}^{film} and K_{eff}^{subs} are the effective inelastic scattering cross sections including the contribution of electrons scattered at depth a inside the film and substrate, respectively, and calculated by formula (15) in [12]; and λ_{eff} is the effective inelastic mean free path of electrons in the bilayer structure. It was assumed in our calculations that the electron inelastic mean free path varies with depth linearly from a value typical of the film material to that typical of the substrate.

The above simulation approach and the MLCS (MultiLayered Cross-Sections) program for computing the inelastic scattering cross section are described in [14]. This program is intended for island films and

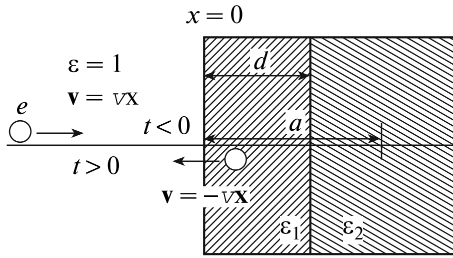

Fig. 4. Geometry of the theoretical model. An electron moving with velocity v from $x = -\infty$ crosses the surface of a solid ($x = 0$) and is mirror-scattered at depth $x = a$ and time instant $t = 0$.

film–interface–substrate systems in which the interface includes the film and substrate materials variously distributed over the depth. To simulate the inelastic scattering cross section, we, according to the Drude–Lindhard model, represented the complex dielectric functions for silicon and iron as a superposition of Lorentz oscillators the parameters of which were found by fitting to our reference silicon and iron spectra.

Figure 5 shows the results of simulation of the inelastic scattering cross section for sample *A* obtained by applying an iron film about 2 nm thick on a Si(100) substrate at room temperature. Curve *1* is the experimental spectrum, and curve *2* is a model spectrum taken of a sharp film–substrate interface for a film thickness of 2.15 nm. It is at this empirically found thickness of the film that the maximum of λK meets an experimental value of 0.0368 eV^{-1}. However, the position of the energy loss maximum differs markedly from the experimental position. Attempts to simulate the inelastic scattering cross section by varying the iron and silicon distributions across the interface (linear, exponential, or uniform) did not result in reasonable agreement between experimental and model data. The energy positions of the maxima of the electron inelastic scattering cross section, which correspond to the excitation of volume plasmons, also disagree with experimental data. Satisfactory agreement between the theory and experiment was obtained only under the double-interface consideration, when an additional silicide layer was introduced with its own dielectric function differing from those of pure silicon and pure iron (Fig. 5, curve *3*).

It was reported [11, 15] that, when an iron film is applied on a silicon substrate at room or low temperature, an iron silicide (FeSi) interfacial layer frequently forms. For thickness *dm* of the interfacial layer and effective cross section $K_{\text{eff}}^{\text{int}}$ of inelastic scattering in the interface, the inelastic scattering cross section of the system is given by

$$K_{sc}(E_0, \hbar\omega) = \frac{1}{\lambda_{\text{eff}}^2}\int_0^d 2a\exp(-2a/\lambda_{\text{eff}})K_{\text{eff}}^{\text{film}}(E_0, \hbar\omega, a)da$$

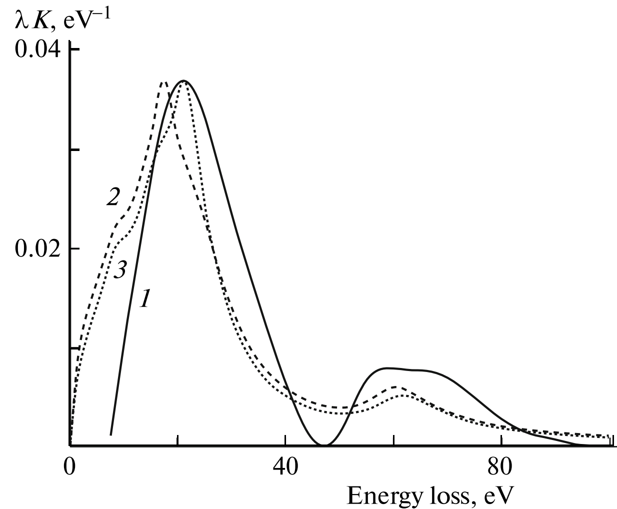

Fig. 5. (*1*) Experimental spectrum of the electron inelastic scattering cross section for sample *A* and model spectra in the case of (*2*) a sharp film–surface interface and (*3*) a monosilicide interfacial layer.

$$+\frac{1}{\lambda_{\text{eff}}^2}\int_d^{d+dm} 2a\exp(-2a/\lambda_{\text{eff}})K_{\text{eff}}^{\text{int}}(E_0, \hbar\omega, a)da \qquad (3)$$

$$+\frac{1}{\lambda_{\text{eff}}^2}\int_{d+dm}^{\infty} 2a\exp(-2a/\lambda_{\text{eff}})K_{\text{eff}}^{\text{subs}}(E_0, \hbar\omega, a)da.$$

As in the first case, the effective inelastic mean free path of electrons is a linear function of the above quantities in the film, interface, and substrate. For iron silicides, the inelastic mean free path of electrons was interpolated in accordance with the iron-to-silicon volume concentration ratio.

The parameters of Lorentz oscillators were simulated by modifying them for pure silicon so that the maximal product of the electron inelastic mean free path by the inelastic scattering cross section was 0.0544, which corresponds to the $Fe_{0.5}Si_{0.5}$ composition in the calibration curve (Fig. 3), and the energy position of the maximum of this product was close to the mean published value [11] for the energy of a volume plasmon in iron monosilicide (20.9 eV). Using these parameters, we achieved the best agreement for the structure Fe(1.3 nm)/FeSi(2.5 nm)/Si(100). The effective thickness of the iron layer in this case is 2.5 nm, which somewhat exceeds the technological value (2.0 nm).

For sample *B* grown at a substrate temperature of 270°C, we failed in simulating a spectrum of inelastic scattering cross sections assuming that the interface consists of iron monosilicide only. The experimental value of the maximal product of the electron inelastic mean free path by the inelastic scattering cross section for this sample was larger than for iron monosilicide. Therefore, to correctly treat experimental data, we

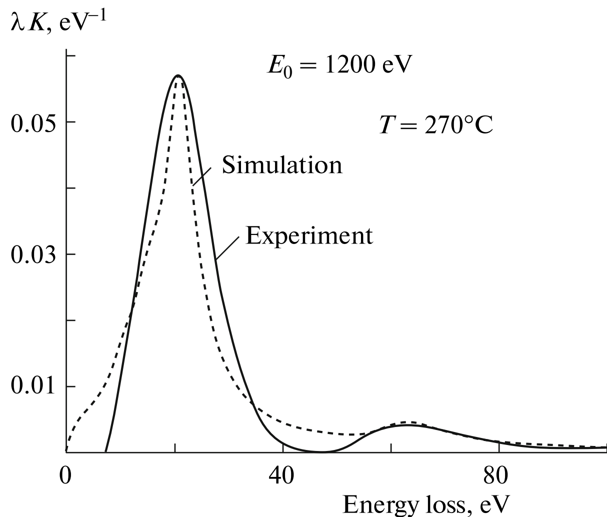

Fig. 6. Experimental and theoretical spectra of the electron inelastic scattering cross section for sample *B* grown at a substrate temperature of 270°C.

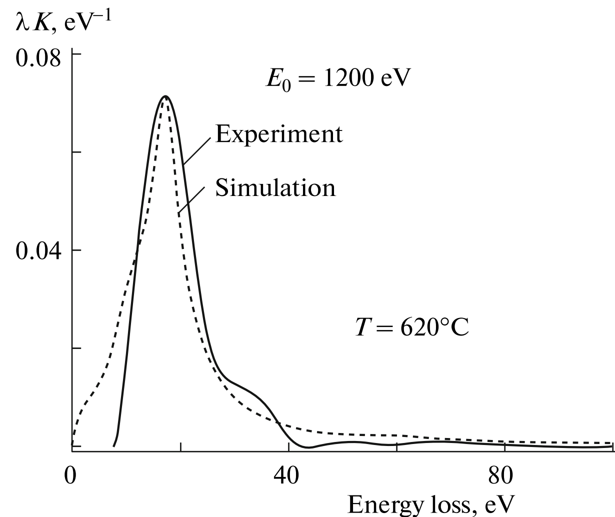

Fig. 7. Experimental and theoretical spectra of the electron inelastic scattering cross section for sample *E* grown at a substrate temperature of 620°C.

had to consider the influence of iron disilicide (which forms at higher temperatures according to publications) on the model spectra. As for the monosilicide, the parameters of Lorentz oscillators for pure silicon were modified so that the maximum of λK corresponded to the $Fe_{0.34}Si_{0.66}$ composition with a plasmon energy of 20.6 eV. The best agreement was achieved for the upper homogeneous iron monosilicide + iron disilicide layer with volume fractions of 0.64 and 0.36, respectively (Fig. 6).

For the samples obtained at 620°C, the iron content is less than 30 at % and depends on growth conditions. At such a low iron concentration in the subsurface layer, it seems unlikely that the silicide content will be high. This is also indicated by the experimental values of the volume plasmon energy (Table 1), which coincide with the plasmon energy for pure silicon accurate to a measurement error. Presumably, due to the very fast diffusion of iron atoms into the silicon substrate, a sufficiently thick layer (with a thickness of this layer far exceeding the inelastic mean free path of electrons) of iron–silicon solid solution arises. Based on this assumption, we simulated a spectrum of the inelastic scattering cross section for samples *C*, *D*, and *E*, considering them as homogeneous silicon–iron composites.

Figure 7 shows the experimental spectrum of the inelastic scattering cross section for sample *E*, in which the iron concentration is the lowest, and a spectrum obtained by simulating the uniform distribution of silicon and iron with volume concentrations of 90.7 and 9.3%, respectively. The deviation from the volume concentration of silicon for this sample (Table 2), which was calculated from the atomic concentration in accordance with the calibration curve (Fig. 3), equals 1.1%.

CONCLUSIONS

New opportunities for quantitative analysis of the elemental composition, chemical state, element distribution across the depth, and formation of different silicide phases using the computer simulation of the electron inelastic scattering cross section is demonstrated with Fe/Si(100) nanostructures obtained under various growth conditions.

ACKNOWLEDGMENTS

The authors thank S.N. Varnakov for assistance in experiments.

This work was supported by the analytical target program "Development of Scientific Potential of Higher School" (project no. 2.1.1.3656); integration project at the Siberian and Far East Branches, Russian Academy of Sciences; program "Spintronics," Department of Physical Sciences, Russian Academy of Sciences; and federal target program "Scientific and Scientific–Pedagogical Personnel of Innovative Russia 2009–2013."

REFERENCES

1. B. Egert and G. Panzner, Phys. Rev. B **29**, 2091 (1984).
2. J. M. Gallego and R. Miranda, J. Appl. Phys. **69**, 1337 (1991).
3. J. M. Gallego, J. M. Garcia, J. Alvarez, et al., Phys. Rev. B **63**, 13339 (1992).
4. M. V. Gomoyunova, I. I. Pronin, D. E. Malygin, et al., Zh. Tekh. Fiz. **75** (9), 106 (2005) [Tech. Phys. **50**, 1212 (2005)].
5. M. V. Gomoyunova, D. E. Malygin, and I. I. Pronin, Fiz. Tverd. Tela (St. Petersburg) **48**, 1898 (2006) [Phys. Solid State **48**, 2016 (2006)].

6. L. Wang, C. Lin, Q. Shen, et al., Appl. Phys. Lett. **66**, 3453 (1995).

7. A. S. Parshin, G. A. Aleksandrova, A. E. Dolbak, et al., Pis'ma Zh. Tekh. Fiz. **34** (9), 41 (2008) [Tech. Phys. Lett. **34**, 381 (2008)].

8. S. N. Varnakov, A. A. Lepeshev, S. G. Ovchinnikov, et al., Prib. Tekh. Eksp., No. 6, 125 (2004).

9. S. Tougaard, http://www.quases.com.

10. S. Tougaard and I. Chorkendorff, Phys. Rev. B **35**, 6570 (1987).

11. V. G. Lifshits and Yu. V. Lunyakov, *EELS (Electron Energy Loss Spectroscopy) Spectra of Surface Phases in Silicon* (Dal'nauka, Vladivostok, 2004) [in Russian].

12. F. Yubero and S. Tougaard, Phys. Rev. B **46**, 2486 (1992).

13. A. S. Parshin, S. A. Kushchenkov, and G. A. Aleksandrova, in *Proceedings of the 3rd International Conference on Physics of Electronic, Kaluga, 2008*, Vol. 1, pp. 231–234.

14. S. A. Kushchenkov, A. S. Parshin, G. A. Aleksandrova, and S. A. Khodenkov, Vestn. Sib. Gos. Aerokosm. Univ. im. M. F. Reshetieva, No. 4 (25), 129 (2009).

15. M. Schleberger, Surf. Sci. **445**, 71 (2000).